IEEE Access
Multidisciplinary | Rapid Review | Open Access Journal

Received 13 July 2024, accepted 19 July 2024, date of publication 29 July 2024, date of current version 6 August 2024.

Digital Object Identifier 10.1109/ACCESS.2024.3434554

APPLIED RESEARCH

Design of a Cascade Control Scheme for Unwinding Tension Based on RBF Network

LIANG WANG[1], HENGSHENG WANG[1,2], ZHOU OUYANG[1], HUA LIU[1], AND ZEXING ZHENG[1]

[1]College of Mechanical and Electrical Engineering, Central South University, Changsha 410083, China
[2]State Key Laboratory of High Performance Complex Manufacturing, Central South University, Changsha 410083, China

Corresponding author: Hengsheng Wang (whscsu@163.com)

This work was supported in part by the National Natural Science Foundation of China under Grant 51975587, and in part by Shenzhen Gade Equipment Technology Company Ltd.

ABSTRACT In the working process of the diaphragm slitting machine, a cascade control scheme based on the RBF network is proposed to address the tension fluctuation problem caused by the nonlinearity, strong coupling, and parameter variation of the unwinding system. Firstly, the dynamic characteristics of the unwinding process of the diaphragm slitting machine are analyzed, and the dynamic model of the unwinding section is established. The influencing factors causing tension fluctuation are studied. Then, a cascade control strategy combining sliding mode control (SMC) and RBF network adaptive sliding mode control (RBF-ASMC) is proposed to hierarchically control the key variables of unwinding tension and unwinding speed, which are coupled with each other. The sliding mode controller ensures stable control of the outer tension loop, and the RBF network adaptive sliding mode controller adds disturbance compensation and robust control to the inner speed loop. Finally, simulation and experimental results demonstrate that the cascade control scheme based on the RBF network weakens the coupling between key variables in the system, improves the dynamic performance, and enhances the disturbance rejection capability of the system.

INDEX TERMS Tension control, speed control, RBF network, adaptive sliding mode control, cascade control.

I. INTRODUCTION

Diaphragm is a kind of web used in lithium-ion batteries as a separator between positive and negative materials. Diaphragm slitters are usually deployed to convert a large-width diaphragm roll into multi-smaller rolls, which is a common web processing technique through roll-to-roll(R2R) transportation. It is very important to keep the web tension in a delicate range during slitting, which is of great influence on the quality of final rewound rolls. The tension of the unwinding section comes as the base tension of the moving web in the machine direction, which is critically important to guarantee the proper slitting process and the final rewinding of the roll. The thickness of the diaphragm is about several micrometers to a few dozen micrometers, and having a trend of being thinner; Improper tension easily causes bad effects, as wrinkle, slack, rupture, or lateral movement, which influences the slitting quality and then the rewinding quality; the fluctuation of unwinding tension may also transfer to downstream sections and have bad consequences on the product. This work mainly concerns the tension control problem in the unwinding span of a diaphragm slitter.

In web tension control, speed and tension are two of the most important control variables. To achieve decoupled or coordinated control of speed and tension, extensive and in-depth research has been conducted by experts and scholars both domestically and internationally. In [1], the Kalman filter was applied to the online filtering of sensor measurement signals in roll-to-roll systems, and the tension control performance was improved by combining feedforward and disturbance compensation. In [2], a multivariable sliding mode surface was designed to balance the unwinding

The associate editor coordinating the review of this manuscript and approving it for publication was Jinquan Xu.

tension and speed in roll-to-roll systems, and tension control during unwinding was achieved using sliding mode control under servo system torque mode. In [1] and [2], the torque control of unwinding tension as a single variable constrains the improvement of control accuracy. In [3], a more comprehensive tension control model for the winding process was proposed, which considered both the web tension and the transmission speed to achieve precise control of winding tension for high-speed small tension tape transfer machines. In [4], an H_∞ control strategy and a linear parameter varying (LPV) strategy were applied for the control of tension and transport velocity. The system dynamics were linearized around the operating point and the change in rolling radius is handled specially. In [5], they considered factors such as the complexity of the process, which may cause variations in material elastic modulus, unwinding radius, and rotational inertia, as well as constraints on control variables imposed by complex operating environments. They used a linear parameter-varying model predictive control (LPV_MPC) to enhance the tension tracking performance of the tension controller and used an increment model to eliminate the error between the nominal and actual models. In [6], a decentralized linear quadratic control strategy was proposed to regulate the transmission speed and web tension. The drawback of the methods in [3], [4], [5], and [6] is that their linear controllers are only effective within a limited range of states of the nonlinear roll-to-roll system due to linearization. In [7] and [8], on the basis of using cascade control for web tension and transmission speed, a tension observer was introduced, and the observed value was used as the pre-feedback compensation of the system input, which has good robustness and dynamic response performance. However, this observer did not accurately estimate nonlinear disturbances. Moreover, the control strategy of controlling tension through speed difference is widely accepted in the winding industry, but it is unstable and easily affected by sudden disturbances and initial errors during adjustment or tracking. Therefore, this naturally leads to the need for a new feedback or closed-loop control algorithm that can simultaneously stabilize unwinding tension and unwinding speed while considering the effects of nonlinear disturbances.

However, despite extensive research, tension control during the unwinding process is not easy due to time-varying parameters and external interference, as well as the increasing speed of unwinding. Neural networks (NN) have been widely used as effective methods to overcome model uncertainty and external disturbances. In [9], Lewis first proposed the use of neural network approximation for compensating external disturbances in the control of a two-link robotic arm in 1996, providing a theoretical basis for the subsequent application of neural networks. In [10], a PID controller based on the BP neural network was proposed for the unwinding system, and the neural network control theory and PID control algorithm were adjusted based on the nonlinearity and time-varying characteristics of the unwinding system. In [11], an adaptive RBF network was proposed to design an approximation function for the disturbance, compensating for disturbances in the control law of the continuous robust integral of the sign of the error (RISE) controller, and its effectiveness was verified through experimental analysis. In [12] and [13], neural network was used to compensate unknown dynamics, respectively for DC motor and hydraulic manipulator, and the control systems' performance was guaranteed accordingly. In [14], the proposed approximate optimal tracking control framework had a more general application scenario, which could optimize the performance using the part of the system dynamics that might be known while the prescribed performance was guaranteed, and compensated for the unknown part of the system dynamics by using adaptive NN in the actual controller to obtain better comprehensive performance.

Sliding mode control (SMC) is a suitable control method for the unwinding system due to its ability to overcome disturbances and uncertainties in the system [15], [16], [17]. In [15], a dynamic sliding mode controller was designed based on the power exponent reaching approach law, taking into account the load disturbances, parameter perturbations, and unmodeled dynamics on the speed and tension system of a reversible cold strip mill. The proposed control method can ensure the asymptotic stability of the closed-loop system and effectively reduce system chattering. In [16] and [17], the advantages of sliding mode control were demonstrated, which had strong robustness against modeling uncertainty and external disturbances. However, in the face of many uncertainties in the unwind system, it is difficult to achieve satisfactory control results solely based on the robustness of sliding mode control, and the large gain of the robust term can easily cause chattering.

Considering the uncertainty of the dynamics and nonlinear nature of the unwinding system of the slitter, this paper proposes a cascade control scheme with the inner loop of sliding mode control based on the RBF network for parameter adaptation. The main contributions are as follows:

1) A cascade control method is proposed to address the tension fluctuation problem during the unwinding process of the diaphragm slitting machine. The outer primary control is used to adjust the web tension, while the inner secondary loop is used to control the speed of the unwinding servo motor; An inner loop speed controller with shorter lag and faster response can weaken or eliminate the influence of interference, ultimately reducing its impact on unwinding tension and accelerating the response of the system.

2) The most influential uncertainty in the unwinding system is its frictional torque, which is isolated mainly inside the inner loop by introducing the proposed RBF network based sliding mode speed control; and the control performance of the unwinding tension in the outer loop is then improved.

3) The other uncertainties and disturbances, like properties of the diaphragm, measurement noise of the radius of the

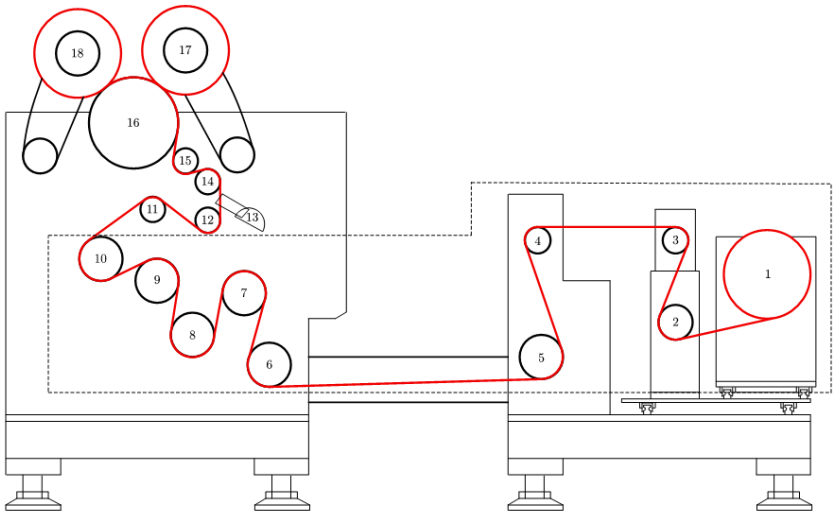

1-Unwinding roll 2,3,4,5,11,12,14,15-Idle roll 5-Load cell 6,7,8,9,10-Pulling roll
13-Knife shaft, fixed straight knife for this machine 16-Master speed roll 17,18-Surface rewinding roll

FIGURE 1. Schematic diagram of the diaphragm slitter.

unwinding roll, etc., can be taken care of by the outer sliding mode control. The whole system stability of the designed cascade control algorithm has been theoretically proven, and the superiority of this method has been demonstrated with simulation and experimental results.

Following this introduction, section II introduces the experimental platform, system modeling, and the goals of improving disturbance resistance and dynamic performance of tension control. Section III focuses on torque control of the unwinding motor, using the Lyapunov function as the stability criterion, and designing a cascaded controller combining sliding mode control with RBF network adaptive sliding mode control. In Sections IV and V, through simulation and experiments, the designed cascaded controller demonstrates good control performance of diaphragm tension in the unwinding system and adaptability to complex operating conditions.

II. SYSTEM MODELING

Fig. 1 shows the schematic diagram of the diaphragm slitter mentioned in this paper. There are three motor drives, unwinding roll 1, pulling drive of group rolls 6,7, 8, 9, 10, and primary speed roll 16; others are idle rollers, including roller 5 with a load cell for tension measurement; 17 and 18 are surface rewinding rolls. There is no nip allowed in the slitter to avoid the possibility of damaging to diaphragm surface. Because of the s-wrap of the pulling rolls the unwinding tension zone can be considered independent of downstream sections under some proper assumptions. The primary servo drive sets the transporting speed (or primary speed) of the web in the velocity mode of servo control, and the pulling drive is also in velocity mode with a manual-adjustable speed ratio to the speed of the primary drive. With the consideration of the dependence of the unwinding tension zone, we think of the speed of the pulling roll being a known term, and the control of unwinding tension is the job of controlling the servo drive of the unwinding roll.

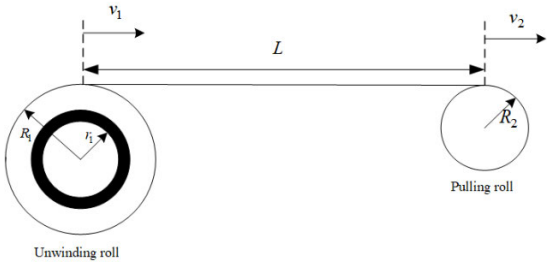

FIGURE 2. Simplified schema of the unwinding tension zone.

A. DYNAMICS OF WEB TENSION

The simplified schema of the unwinding tension zone is provided in Fig. 2. The dynamics of web tension in the unwinding span can be expressed in (1) [2], [6], [22]. The following assumptions were made for the sake of simplification: 1) the inertia and friction of the idle rolls are relatively small, and can be neglected in modeling; 2) the web strain is elastic; 3) the web slipping is neglected.

$$\dot{T}_1 = -\frac{v_2}{L}T_1 + \frac{(T_0 - EA)\,R_1}{L}\dot{\theta}_1 + \frac{EA}{L}v_2 \tag{1}$$

where T_1 is the web tension, T_0 is the inside tension of the original web roll, R_1 is the outer radius of the material roll, E is the modulus of elasticity of the web material, A is the cross-sectional area of the web, L is the length of the web span between the unwinding roll and the pulling roll, v_1 is the linear speed of the unwinding roll, v_2 is the linear speed of the pulling roll.

At the equilibrium point, i.e., $\dot{T}_1 = 0$, the web tension is,

$$T_1 = EA\left(1 - \frac{v_1}{v_2}\right) + \frac{v_1}{v_2}T_0 \tag{2}$$

and the dynamical process of the tension is governed by,

$$T_1(t) = T_0 e^{-\frac{v_2}{L}t} + (1 - e^{-\frac{v_2}{L}t}) \times [EA(1 - \frac{v_1}{v_2}) + \frac{v_1}{v_2}T_0] \tag{3}$$

We can see that the equilibrium tension of the system is determined by the ratio of the linear speed between the unwinding roll and the pulling roll, and the dynamical process in this first-order system is determined by the time constant ($\tau = L/v_2$) which is not a constant but variable with the primary speed of the web transportation.

If we put $T_0 = 0$, and define strain $\varepsilon = 1 - v_1/v_2$, a positive number much less than 1, we have,

$$T_1 = EA\varepsilon \tag{4}$$

The typical static strain-stress curve of the diaphragm looks like Fig. 3(a), which shows the nonlinear nature of Young's modulus of the web; and a proper coordinate transformation gives Fig. 3(b) which shows the static curve of tension as a nonlinear function of speed ratio according to (2) when $T_0 = 0$.

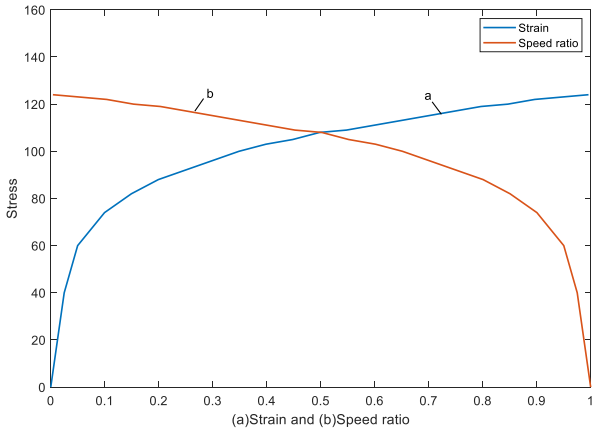

FIGURE 3. (a) Typical strain-stress curve of diaphragm; (b) Static curve of tension as a function of speed ratio.

B. DYNAMICS OF UNWINDING DRIVE

The typical belt transmission of unwinding drive is shown in Fig. 4. To get some desired unwinding tension T_r, we must give desired linear velocity v_r as follows,

$$v_r = \frac{(T_r - EA)v_2}{T_0 - EA} \tag{5}$$

But we would not have precise v_r to give, because there are uncertainties on T_0 and E in (5); furthermore, we would not have precise v_r to get, because $v_r = \dot{\theta}_r R_1$ and the variate R_1 could not easily be precisely obtained.

We would have not cared about v_r, because there is a direct torque balance related to the unwinding tension T_1 on the drive's side as follows [2], [6], [22]:

$$\frac{d}{dt}(J_1\dot{\theta}_1) = R_1 T_1 + i\tau_1 - b\dot{\theta}_1 \tag{6}$$

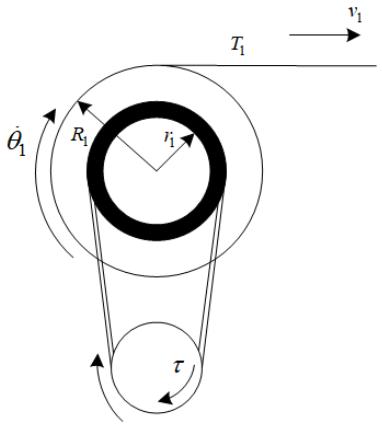

FIGURE 4. Cross-sectional view of the unwinding drive.

where $\dot{\theta}_1$ is the angular speed of the unwinding roll, J_1 is the inertia of the unwinding section, τ_1 is the input torque from the unwinding motor, b is the coefficient of friction, i is the transmission ratio.

J_1 is time-variable, which consists of three parts:

$$J_1(t) = i^2 J_m + J_c + J_w(t) \tag{7}$$

where J_m is the inertia of all the rotating elements on the motor side, which includes inertia of motor armature, driving pulley, driving shaft; J_c is the inertia of the driven shaft and the core mounted on it, and $J_w(t)$ is the inertia of the web material on the core. During the unwinding process, the diameter of the material roll decreases until the end of the process, $J_w(t)$ is time-varying:

$$J_w(t) = \frac{\pi}{2}\rho H(R_1^4 - r_1^4) \tag{8}$$

where r_1 is the inner radius of the material roll, H and h are the width, and thickness of the web, ρ are the density of the web material. Therefore, Equation (6) can be written as:

$$\dot{J}_1\dot{\theta}_1 + J_1\ddot{\theta}_1 = R_1 T_1 - i\tau_1 - b\dot{\theta}_1 \tag{9}$$

Taking the derivative of J_1 yields:

$$\dot{J}_1 = 2\pi\rho H R_1^3 \dot{R}_1 \tag{10}$$

Due to the small thickness of the diaphragm compared to the radius of the material roll, the rate of change of radius R_1 is approximately as follows:

$$\frac{dR_1}{dt} = -\frac{h\dot{\theta}}{2\pi} \tag{11}$$

Equation (9) can be simplified as:

$$\ddot{\theta}_1 = \frac{R_1}{J_1}T_1 + \frac{1}{J_1}i\tau_1 - \frac{b}{J_1}\dot{\theta}_1 - \frac{\rho H R_1^3}{J_1}h\dot{\theta}_1^2 \tag{12}$$

The whole dynamics for the tension system of the unwinding section consists of (1), (7), (8), (11) and (12).

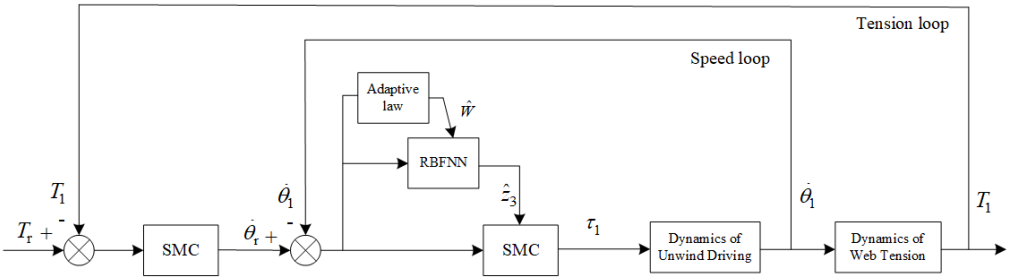

FIGURE 5. Unwinding tension control scheme.

III. THE CASCADE CONTROL SYSTEM DESIGN

The unwinding tension control scheme is shown in Fig. 5, using a cascade control structure [23], [24], [25]. The outer primary control is used to adjust the web tension. The inner secondary loop is for the speed control of the unwinding servo motor, which is to track the reference speed given by the primary controller. Disturbances in the inner loop are approximated and compensated in real time using an RBF network.

A. DESIGN OF OUTER LOOP CONTROLLER

A sliding mode controller is designed with the web tension dynamic model, which can be obtained from (1):

$$\dot{T}_1 = -\frac{v_2}{L}T_1 + \frac{(T_0 - EA)\,R}{L}\dot{\theta}_1 + \frac{EA}{L}v_2 + d_1 \tag{13}$$

Let

$$x = T_1, u_1 = \dot{\theta}_1, g_1 = \frac{(T_0 - EA)R_1}{L}, f_1 = \frac{(EA - T_1)}{L}v_2$$

Equation (13) can be simplified to

$$\dot{x} = g_1 u_1 + f_1 + d_1 \tag{14}$$

where d_1 is the disturbance of the outer loop. Disturbances in engineering are bounded, let $|d_1| \le k_2$, $k_2 > 0$.

For the first-order dynamic model of web tension, the following sliding mode function is introduced,

$$s_1 = c_1 e_1 \tag{15}$$

where $c_1 > 0_\circ$

The tracking error is $e_1 = T_r - x$, where T_r is the reference tension.

Define the Lyapunov function as,

$$V = \frac{1}{2}s_1^2 \tag{16}$$

And,

$$\begin{aligned}\dot{s}_1 &= c_1\dot{e}_1 = c_1\left(\dot{T}_r - \dot{x}\right)\\ &= c_1\left(\dot{T}_r - gu_1 - f(x) - d_1\right)\end{aligned} \tag{17}$$

In order to ensure $s_1\dot{s}_1 \le 0$, the sliding mode control law can be designed as,

$$u_1 = \frac{1}{g}\left(\dot{T}_r - f(x) + k_1 s_1 + k_2 \tanh s_1\right) \tag{18}$$

where $k_1 > 0_\circ$ In equation (18), the discontinuous symbolic function $\mathrm{sgn}s_1$ is replaced by hyperbolic tangent function $\tanh s_1$, which is defined as,

$$\tanh s_1 = \frac{e^{s_1} - e^{-s_1}}{e^{s_1} + e^{-s_1}}$$

Then,

$$\begin{aligned}\dot{s}_1 &= c_1\left(\dot{T}_r - \left(\dot{T}_r - f(x) + k_1 s_1 + k_2 \tanh s_1\right)\right.\\ &\left. - f(x) - d_1\right) = -c_1\left(k_1 s_1 + k_2 \tanh s_1 + d_1\right)\end{aligned} \tag{19}$$

So,

$$\begin{aligned}\dot{V} &= s_1\dot{s}_1 = -c_1\left(k_1 s_1^2 + k_2|s_1| + d_1 s_1\right) \le -c_1 k_1 s_1^2\\ &= -\frac{c_1 k_1}{2}V\end{aligned} \tag{20}$$

The solution to the inequation $\dot{V} \le -\frac{c_1 k_1}{2}V$ is,

$$V(t) \le e_1^{-\frac{c_1 k_1}{2}(t - t_0)}V(t_0) \tag{21}$$

It can be seen that when $V(t)$ exponentially converges to 0, then s_1 exponentially converges to 0, and the convergence speed depends on $c_1 k_1$, ultimately reaching the reference tension. Therefore, the outer tension loop controller is asymptotically stable, and the system error will converge to 0. The control law u_1 obtained by the outer loop controller will be used as the reference angular speed of the inner loop.

B. DESIGN OF INNER LOOP CONTROLLER

Due to the strong coupling relationship between unwinding tension and unwinding speed, only controlling unwinding tension restricts the improvement of control precision. Therefore, RBFASMC is used to increase disturbance compensation and robust control for the speed loop [26].

1) DESIGN OF SMC CONTROLLER

According to (12), the dynamic of unwinding drive under interference is as follows:

$$\ddot{\theta}_1 = \frac{R_1}{J_1}T_1 + \frac{1}{J_1}i\tau_1 - \frac{b}{J_1}\dot{\theta}_1 - \frac{\rho H R_1^3}{J_1}h\dot{\theta}_1^2 + d_2 \tag{22}$$

Let the state vector $z = [z_1, z_2, z_3]^T = [\theta_1, \dot{\theta}_1, d_2]^T$, where $\theta_1, \dot{\theta}_1$ is the actual angle and the angular speed of the unwinding roll, d_2 is the disturbance of the inner loop. Disturbances in engineering are bounded, let $|d_2| \le k_4$, $k_4 > 0$.

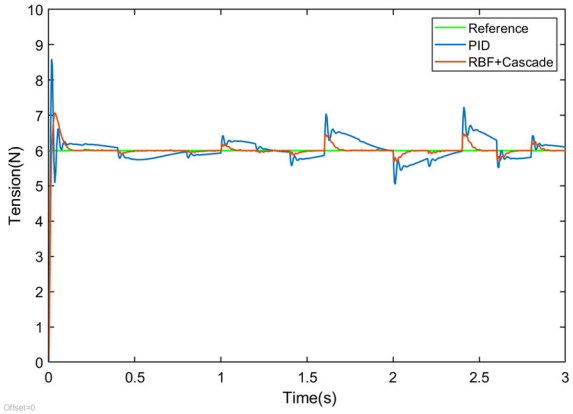

(a) Tension tracking curve

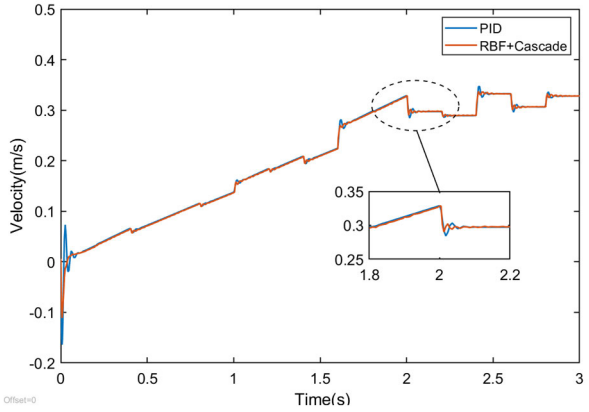

(b) Speed tracking curve

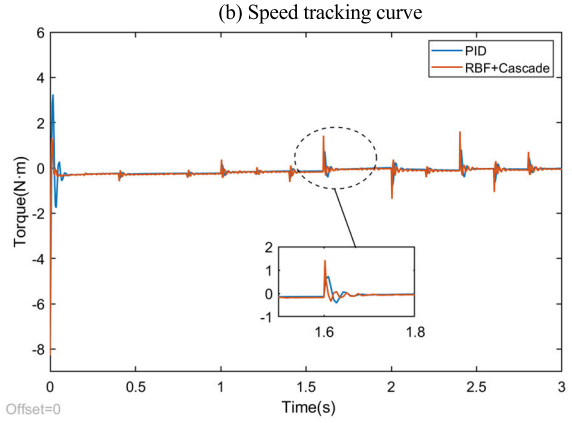

(c) Motor torque curve

FIGURE 6. Comparison of control performance under model parameter errors.

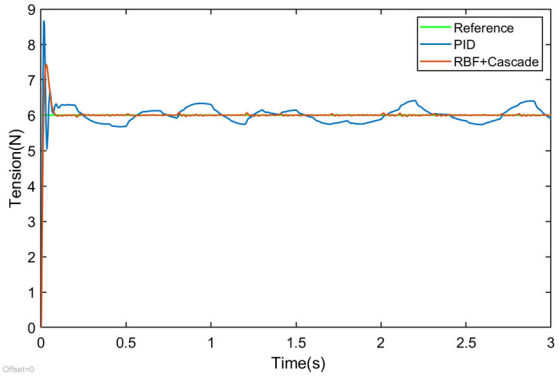

(a) Tension tracking curve

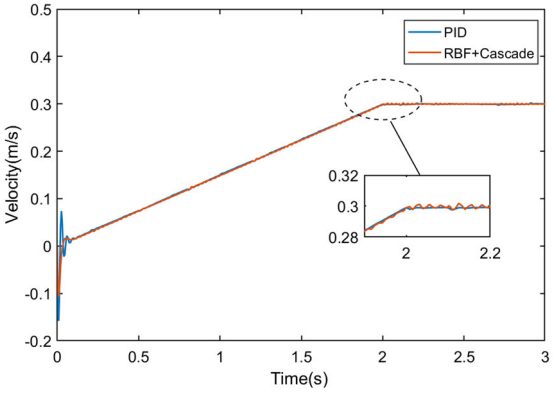

(b) Speed tracking curve

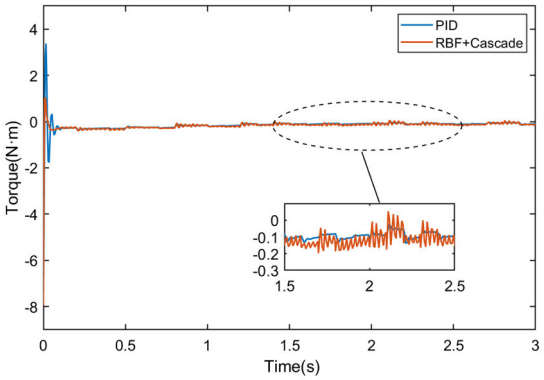

(c) Motor torque curve

FIGURE 7. Comparison of control performance under continuous interference.

τ_1 is the input torque from the unwinding motor. Let $u_2 = \tau_1$, $g_2 = \frac{1}{J_1}, f_2 = \frac{R_1}{J_1}T_1 - \frac{b}{J_1}z_2 - \frac{\rho H R_1^3}{J_1}hz_2^2$, Equation (22) can be simplified to:

$$\begin{cases} \dot{z}_1 = z_2 \\ \dot{z}_2 = i \cdot g_2 u_2 + f_2 + z_3 \end{cases} \tag{23}$$

In order to achieve the inner loop control objective, the design of the RBF network adaptive sliding mode controller is as follows. First, the tracking error of the unwinding angular speed is defined.

$$e_2 = \dot{\theta}_r - z_2 \tag{24}$$

The sliding mode function is defined as:

$$s_2 = e_2 + c_2 \int_0^t e_2 dt \tag{25}$$

where $c_2 > 0$.

Then,

$$\begin{aligned} \dot{s}_2 &= \dot{e}_2 + c_2 e_2 = \ddot{\theta}_r - \dot{z}_2 + c_2 e_2 \\ &= \ddot{\theta}_r - i g_2 u_2 - f_2 - z_3 + c_2 e_2 \end{aligned} \tag{26}$$

In order to ensure $s_2 \dot{s}_2 \leq 0$, the sliding mode control law can be designed as,

$$u_2 = \frac{1}{i \cdot g_2}\left(\ddot{\theta}_r + c_2 e_2 - f_2 - z_3 + k_3 s_2 + k_4 \tanh s_2\right) \tag{27}$$

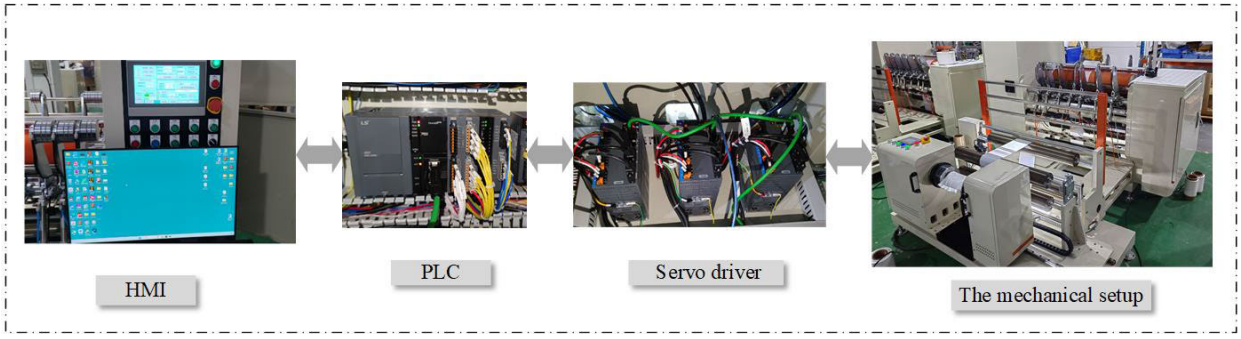

FIGURE 8. The experimental platform.

where $k_3 > 0$, z_3 is the disturbance of the inner loop, which can be approximated online by the RBF neural network, and the approximation value is used as the design basis for the sliding mode controller.

2) RBF NEURAL NETWORK (RBFNN)

Compared with the BP neural network, RBFNN has a simple structure, strong generalization ability, and can approximate any nonlinear function with arbitrary accuracy [18], [19], [20], [21]. RBFNN does not require offline training and can realize online adaptive tuning. Therefore, this paper chooses RBFNN to realize adaptive approximation of disturbances, which can improve the robustness of the controller.

The control algorithm of RBFNN can be described as:

$$\eta_j = \exp\left(\frac{\|\boldsymbol{y} - c_j\|^2}{2b_j^2}\right) \tag{28}$$

$$z_3 = \boldsymbol{W}^{*T}\boldsymbol{\eta}(\mathrm{y}) + \varepsilon \tag{29}$$

where $\boldsymbol{y}$ is the network input vector, η_j is the Gaussian function, $\boldsymbol{W}^*$ is the ideal weight vector, ε is the network approximation error, $|\varepsilon| < \varepsilon_{\max}$, z_3 is the network output, c_j, b_j are the center and width of jth the neuron.

The structure of the RBFNN that we adopt is 1-5-1, that is 1 input node, 5 hidden nodes, and 1 output node. Suppose that the input vector $\boldsymbol{y} = [e_2]$.

The hidden layer output of RBFNN is

$$\eta_j = \exp\left(\frac{\|\boldsymbol{y} - c_j\|^2}{2b_j^2}\right) j = 1, 2, 3, 4, 5$$

The final output of RBF is

$$\hat{z}_3 = \hat{\boldsymbol{W}}^{\mathrm{T}}\boldsymbol{\eta}(\mathrm{y}) \tag{30}$$

where $\hat{\boldsymbol{W}}$ is the actual weight vector. In order to realize the adaptive approximation of $\hat{z}_3$, the adaptive law $\hat{\boldsymbol{W}}$ needs to be adjusted automatically.

The RBF network adaptive sliding mode control law is designed as follows:

$$u_2 = \frac{1}{g_2}\left(-c_2e_2 + \ddot{\theta}_{\mathrm{r}} - f_2 - \hat{z}_3 - k_3s_2 - k_4\tanh s_2\right) \tag{31}$$

3) STABILITY ANALYSIS

Bring (31) into (26),

$$\begin{aligned}\dot{s}_2 &= \ddot{\theta}_{\mathrm{r}} - g_2u_2 - f_2 - z_3 + c_2e_2\\ &= \ddot{\theta}_{\mathrm{r}} - \left(\ddot{\theta}_{\mathrm{r}} + c_2e_2 - f_2 - \hat{z}_3 + k_3s_2 + k_4\tanh s_2\right)\\ &\quad - f_2 - z_3 + c_2e_2\\ &= -\tilde{z}_3 - k_3s_2 - k_4\tanh s_2\end{aligned} \tag{32}$$

where $\tilde{z}_3 = z_3 - \hat{z}_3 = \boldsymbol{W}^{*\mathrm{T}}\boldsymbol{h}(y) + \varepsilon - \hat{\boldsymbol{W}}^{\mathrm{T}}\boldsymbol{h}(y) = \tilde{\boldsymbol{W}}^{\mathrm{T}}\boldsymbol{h}(y) + \varepsilon$,

$\tilde{W} = W^* - \hat{W}_\circ$

The Lyapunov function is designed as

$$L = \frac{1}{2}s_2^2 + \frac{1}{2}\gamma\tilde{\boldsymbol{W}}^T\tilde{\boldsymbol{W}} \tag{33}$$

where $\gamma > 0_\circ$

Refer to (32) and (33), we can obtain

$$\begin{aligned}&\dot{L}\\ &= s_2\dot{s}_2 + \gamma\tilde{\boldsymbol{W}}^{\mathrm{T}}\dot{\tilde{\boldsymbol{W}}} = s_2(-\tilde{z}_3 - k_3s_2 - k_4\tanh s_2) - \gamma\tilde{\boldsymbol{W}}^{\mathrm{T}}\hat{\dot{\boldsymbol{W}}}\\ &= s_2(-\tilde{\boldsymbol{W}}^{\mathrm{T}}\boldsymbol{\eta}(y) - \varepsilon - k_3s_2 - k_4\tanh s_2) - \gamma\tilde{\boldsymbol{W}}^{\mathrm{T}}\hat{\dot{\boldsymbol{W}}}\\ &= -\tilde{\boldsymbol{W}}^{\mathrm{T}}(s_2\boldsymbol{\eta}(y) + \gamma\hat{\dot{\boldsymbol{W}}}) - s_2(\varepsilon + k_3s_2 + k_4\tanh s_2)\end{aligned} \tag{34}$$

Let the adaptive law be

$$\hat{\dot{\boldsymbol{W}}} = -\frac{1}{\gamma}s_2\boldsymbol{\eta}(\mathrm{y}) \tag{35}$$

Then,

$$\dot{L} = -s_2(\varepsilon + k_3s_2 + k_4\tanh s_2) = -k_3s_2^2 - k_4\,|s_2| - s_2\varepsilon$$

Since the RBF network approximation error ε is a small positive real number. Let $k_4 \geq \varepsilon_{\max}$, then $\dot{L} \leq -k_3s_2^2 \leq 0_\circ$

Therefore, according to the stability criterion of the Lyapunov function, it is known that the closed-loop system is asymptotically stable, and the system error will eventually converge to 0.

The above is the design process of the inner loop controller. The description of the RBF network adaptive sliding mode control algorithm is shown in Table 1.

TABLE 1. RBF network adaptive sliding mode control algorithm.

Input e_2
Step 1: Initialize the pre-defined parameters of RBF network.
Step 2: The tracking error is given in (24).
Step 3: The ideal weight vector is given as (35).
Step 4: The hidden layer output of RBF network is given as (28),
Step 5: The final output of RBF network is given as (30),
Step 6: The control law is given as (31).
Step 7: While not converge, return to Step 2.
Output u_2

IV. SIMULATION

To verify the control performance of the designed controller on unwinding tension, a comparison was made between the designed controller and a fixed-gain PID controller based on feedforward compensation through simulation. The system parameters are shown in Table 2, where the friction coefficient and the inertia of the mechanical part were identified through experiments.

TABLE 2. System parameters.

Description	Parameter	Unit	Value
Friction coefficient	b	N/s	0.0529
Modulus of Elastic of the web material	E	N/m^2	1.29×10^9
Width of the web	H	m	0.0605
Length of the span web	L	m	0.57
Thickness of the web	h	m	0.00002
Cross sectional area of the web	A	m^2	1.21×10^{-6}
Inner radius of the material roll	r_1	m	0.0465
Density of the web material	ρ	Kg/m^3	798.7879
Outer radius of the material roll	R_1	m	0.08
Inertia of all the rotating elements on the motor side	J_m	Kg·m^2	0.0102
Inertia of the driven shaft and the core mounted on it	J_c	Kg·m^2	0.000198

To accurately assess the performance of the system, two comprehensive performance indicators are defined from a practical perspective to measure tension tracking performance. I_{APE} is the maximum absolute value of tracking error, which represents the limit performance of the controller; I_{MSE} is the average of the square of the tracking error, which represents the average performance of the controller throughout the entire working cycle. The mathematical expressions for these two indicators are as follows:

$$I_{\mathrm{APE}} = \max_{i=1,\cdots,N} |e(i)|$$

$$I_{\mathrm{MSE}} = \frac{1}{N}\sum_{i=1}^{N}[e(i)]^2$$

where $e(i)$ represents the tension error of the ith sampling point, and N represents the total number of sampling points.

This simulation tested the controller's control effect on unwinding tension and unwinding speed under different operating conditions.

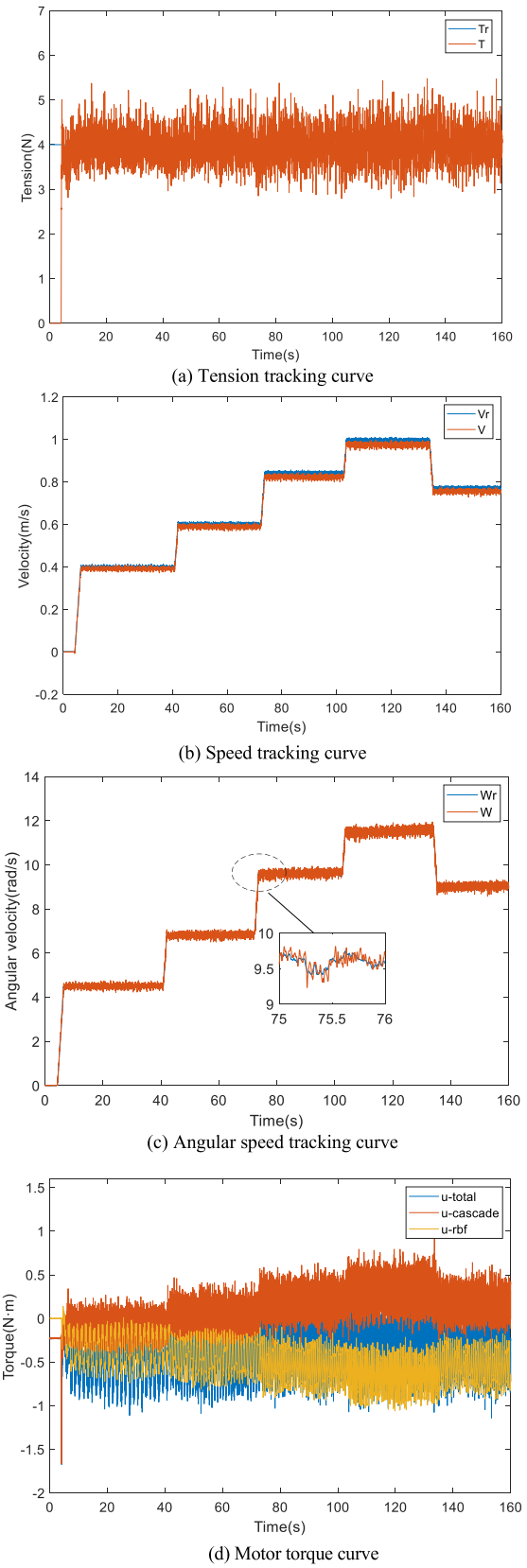

FIGURE 9. Constant tension control experiment with the proposed controller.

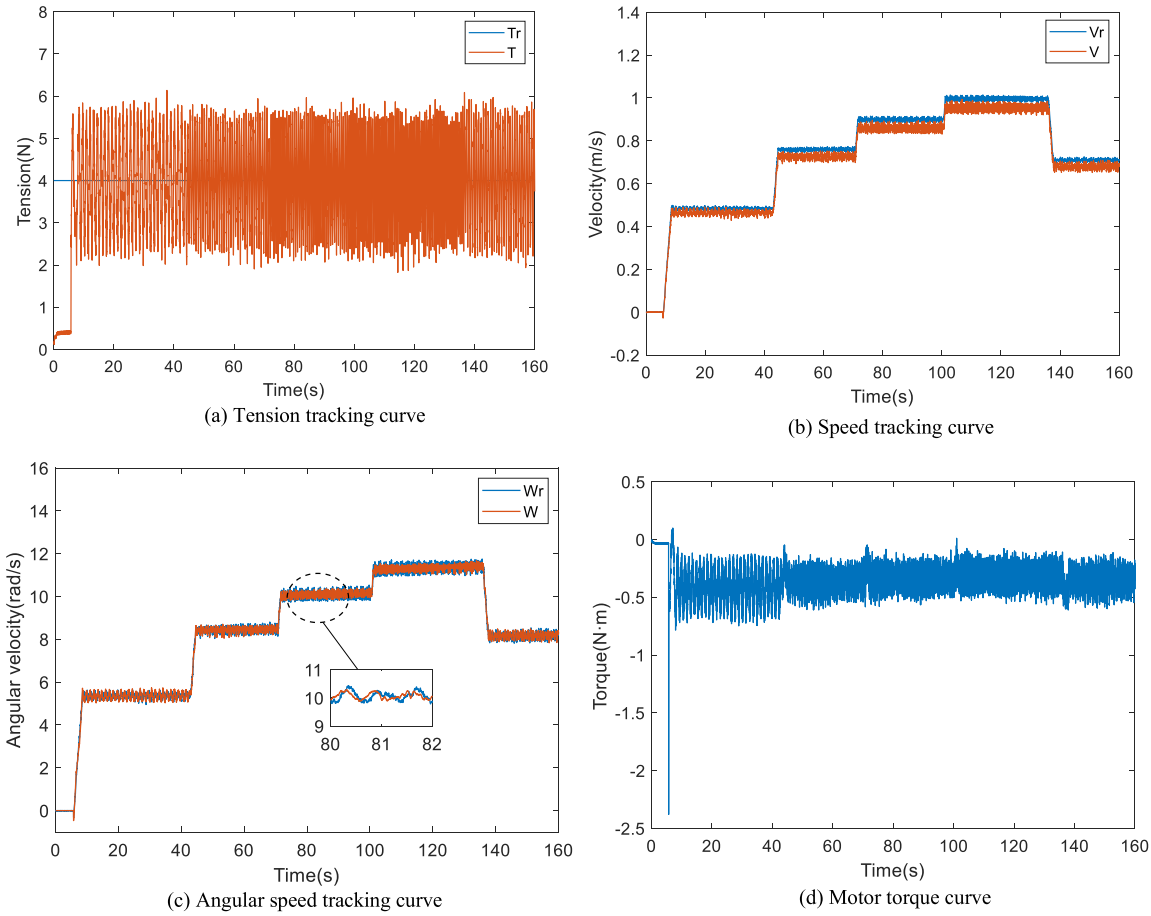

(a) Tension tracking curve
(b) Speed tracking curve
(c) Angular speed tracking curve
(d) Motor torque curve

FIGURE 10. Constant tension control experiment with the cascade controller.

Condition 1: $v_3 = 0.3\text{m/s} v_3 = 0.3\text{m/s}$, $a_3 = 0.15\text{m/s}^2$, $T_r = 6\text{N}$, $R_1(0) = 0.06\text{m}_\circ$

A. MODEL PARAMETER SENSITIVITY SIMULATION

In engineering, it is often difficult to accurately measure the model parameters of an unwinding system. Inaccurate model parameters can affect the control performance of unwinding tension, which requires the controller to be less sensitive to model parameters. Assuming that there is an error of $\pm 0.006\text{m}$ between the measured radius and the actual radius under condition 1, the simulation results are as follows:

As shown in Fig. 6(a) and (b), it can be seen that the web tension response curve under traditional PID control experiences significant fluctuations due to the unwinding radius error, while the web tension response curve under the proposed control has smaller overshoot and fluctuations, faster response speed, and shorter required stabilization time. Relatively speaking, the proposed controller is less sensitive to the accuracy of the model parameters and has better control performance.

B. ANTI-INTERFERENCE SIMULATION

In engineering, there are various uncertain interferences, so it is necessary for the tension controller to have strong anti-interference performance in order to ensure the stability of the tension during the unwinding process. Assuming that the unwinding section under operate condition 1 is continuously disturbed by interference torque within the range of $\pm 0.06\text{N} \cdot \text{m}$, the simulation results are as follows:

As shown in Fig. 7(a) and (b), it can be concluded that under continuous external interferences (randomly within the range of $\pm 0.06\text{N} \cdot \text{m}$), the unwinding tension and unwinding speed under the proposed controller are more stable in both acceleration and steady-state stages, with faster response speed, smaller overshoot, tracking error, and fluctuations.

Moreover, it can be concluded that the proposed controller is suitable for the lithium battery separator slitting machine. It can effectively reduce the overshoot of tension, quickly compensate for speed changes, reduce tension errors, shorten system adjustment time, and demonstrate better disturbance rejection capability.

V. EXPERIMENT

In order to verify the superiority of the control strategy proposed in this paper, we compare the performance of the proposed controller with the cascade controller and PID controller. The experimental platform is shown in Fig. 8,

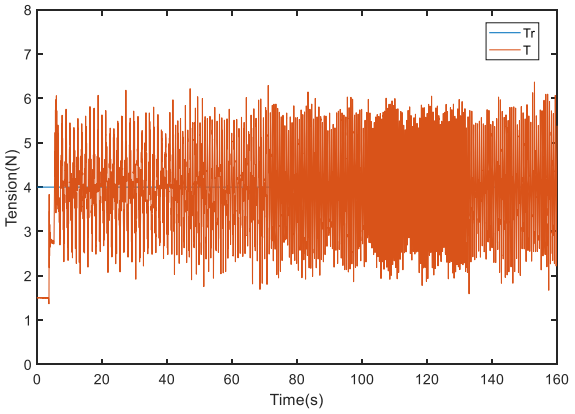

(a) Tension tracking curve

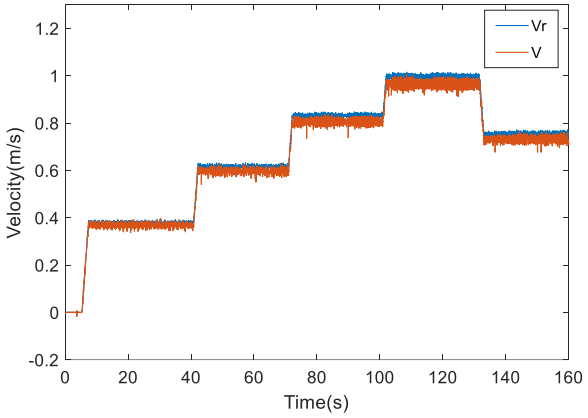

(b) Speed tracking curve

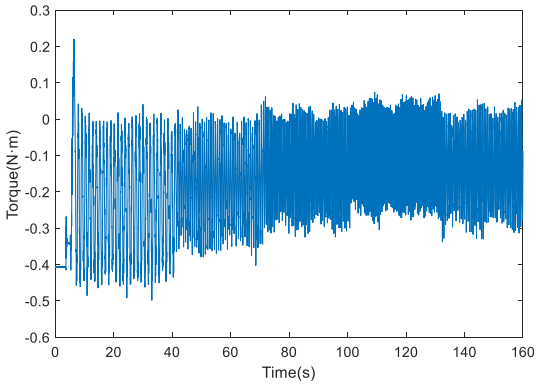

(c) Motor torque curve

FIGURE 11. Constant tension control experiment with the PID controller.

and the comparative experimental results under different conditions are as follows:

Basically, "trial and error" method has been used in the process of experiment. In the proposed controller, the SMC controller parameters are $k_1 = 10, k_2 = 1\mathrm{c}_1 = 200, c_1 = 2$, the RBFASMC controller parameters are $k_3 = 30\mathrm{k}_3 = 30, k_4 = 1, c_2 = 30, \mathrm{c}_2 = 30$ and the RBF network parameters are $b_j = 10, \boldsymbol{c}_j = [-1, -0.5, 0, 0.5, 1], \gamma = 0.001$; The parameters of the cascade controller are $k_1 = 10, k_2 = 1\mathrm{c}_1 = 200, c_1 = 2, k_3 = 30\mathrm{k}_3 = 30, k_4 = 1, c_2 = 30$. The parameters of the PID controller are $k_p = 0.05\mathrm{k}_\mathrm{p} = 1, k_i = 2, \mathrm{k}_\mathrm{i} = 15k_d = 0$.

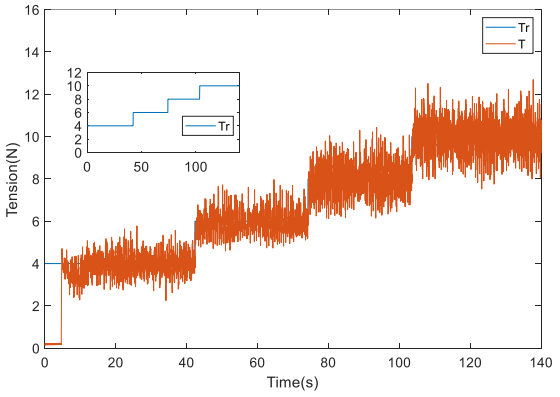

(a) Tension tracking curve

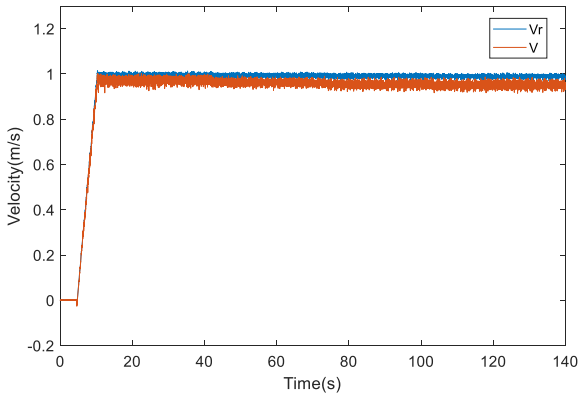

(b) Speed tracking curve

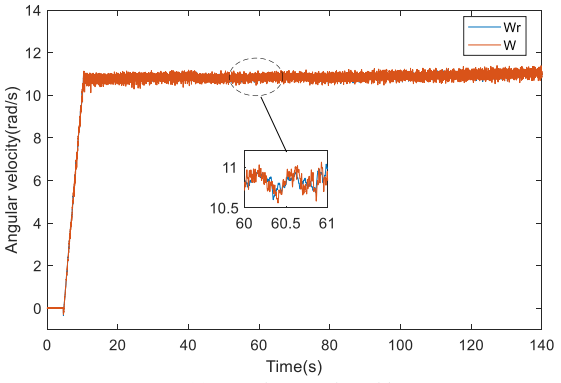

(c) Angular speed tracking curve

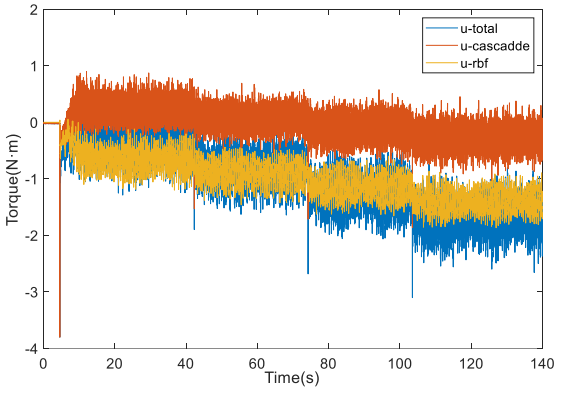

(d) Motor torque curve

FIGURE 12. Variable tension control experiment with the proposed controller.

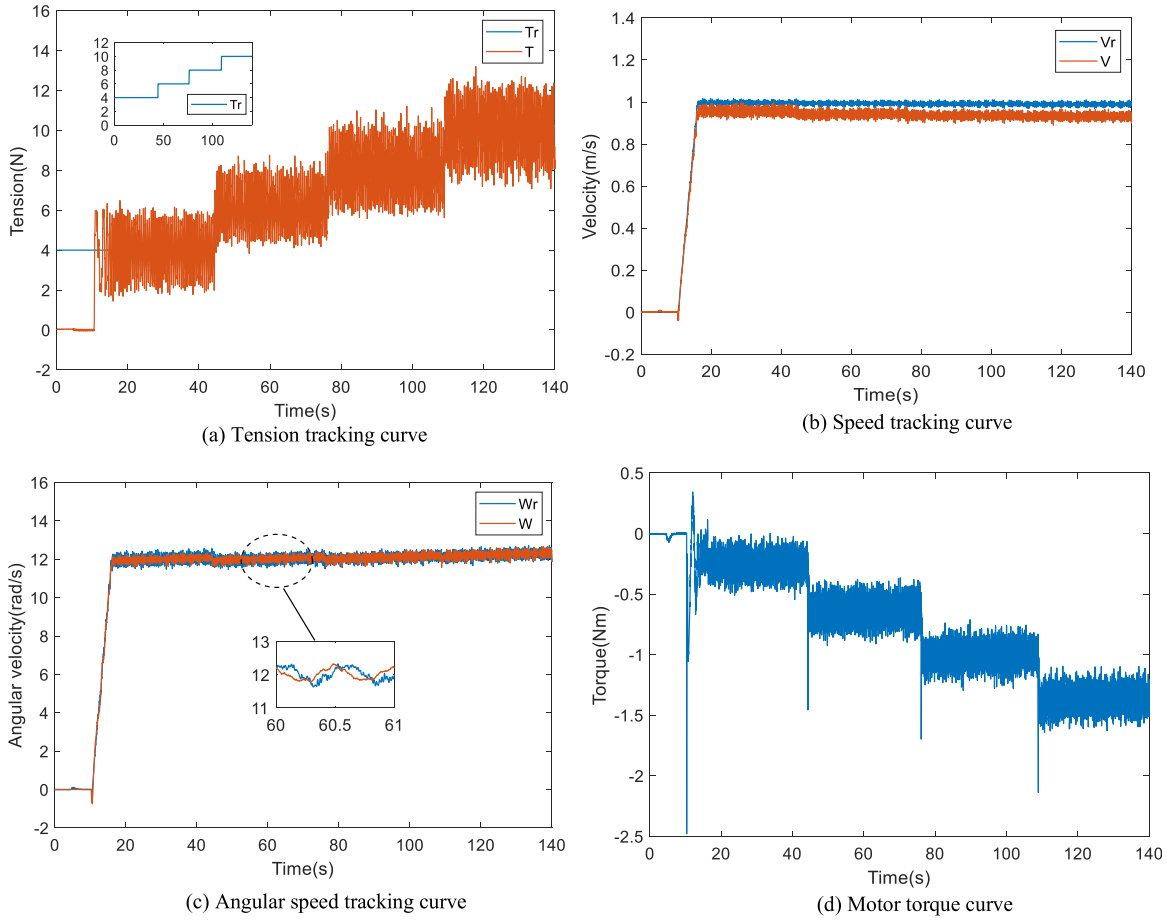

(a) Tension tracking curve
(b) Speed tracking curve
(c) Angular speed tracking curve
(d) Motor torque curve

FIGURE 13. Variable tension control experiment with the cascade controller.

A. CONSTANT TENSION EXPERIMENT

In this experiment, the control effects of different controllers on unwinding tension and unwinding speed were tested under the same reference tension $T_r = 4$N and different transmission speeds (v_2 =0.4m/s to 1m/s, interval 0.2m/s). The reference speed was calculated by (5). The control error indicators in Table 3 and Table 4 are calculated during the steady-state stage.

According to Fig. 9, Fig. 10, Fig. 11, Table 3, and Table 4, it can be seen that the proposed cascade controller has smaller tension steady-state error and better tracking performance. The experiment proves that the designed cascade controller has a good effect on the speed stability of the system.

As shown in Fig. 9(d), the RBFNN output (u-rbf) accounts for most of the proposed controller output (u-total). It can be seen that the RBF network can effectively compensate for the uncertainty of the model and external disturbances, improving the accuracy of the web tension control system.

B. VARIABLE TENSION EXPERIMENT

In this experiment, the control effects of different controllers on unwinding tension and unwinding speed were tested at the same transmission speed $v_2 = 1$m/s and different reference tensions ($T_r = 4$N, 6N, 8N, 10N).

TABLE 3. Tension control error indexes constant tension.

Control Method	I_{APE}	I_{MSE}
PID	2.40	0.94
Cascade	2.18	0.86
Cascade+RBF	1.29	0.12

TABLE 4. Speed control error indexes constant tension.

Control Method	I_{APE}	I_{MSE}
PID	0.094	0.00064
Cascade	0.067	0.00052
Cascade+RBF	0.043	0.00038

As shown in Fig. 12, Fig. 13, Fig. 14, Table 5, and Table 6, the proposed controller has a better tracking effect on the transport speed, so that the steady-state error of the tension is smaller. The proposed controller has better tracking performance and lower steady-state error, and its dynamic behavior and accuracy are better than the cascade controller and PID controller.

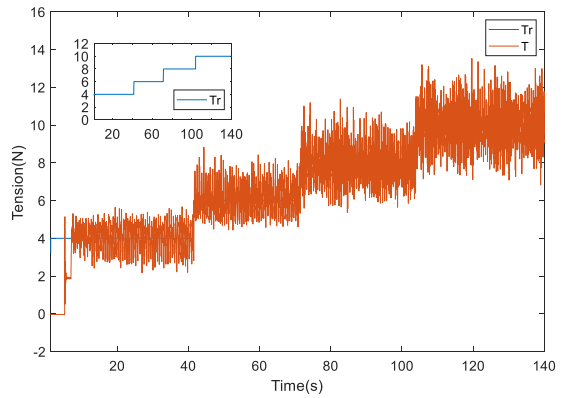

(a) Tension tracking curve

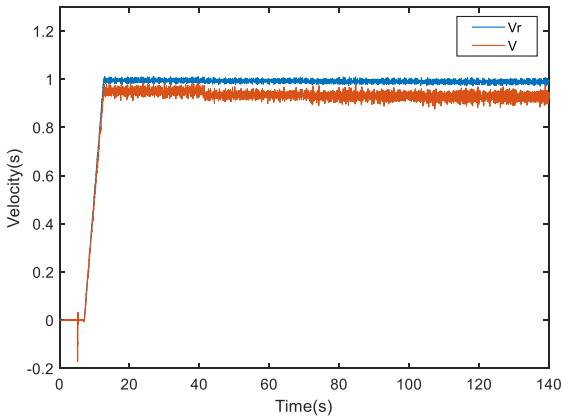

(b) Speed tracking curve

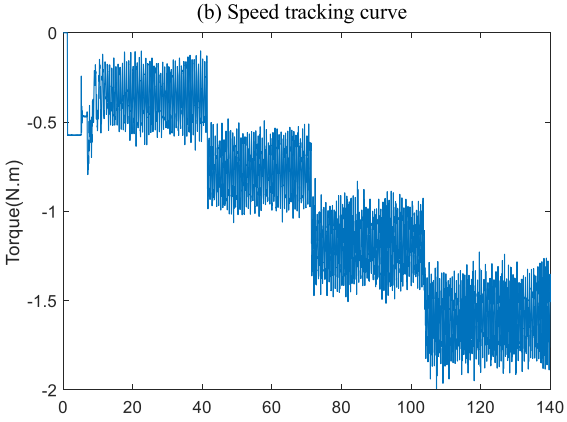

(c) Motor torque curve

FIGURE 14. Variable tension control experiment with the PID controller.

As can be seen from Fig. 12(d), the RBFNN output (u-rbf) accounts for most of the proposed controller output (u-total). It can be seen that the RBFNN can effectively compensate for the uncertainty of the model and external interference, improving the accuracy of the web tension control system.

In summary, the proposed controller in this paper has smaller tracking errors, more stable acceleration and deceleration, and overall better control performance compared to the cascade controller and PID controller. It can be better applied in industrial production.

TABLE 5. Tension control error indexes at variable tension.

Control Method	I_{APE}	I_{MSE}
PID	3.53	0.80
Cascade	3.21	0.52
Cascade+RBF	2.69	0.40

TABLE 6. Speed control error indexes at variable tension.

Control Method	I_{APE}	I_{MSE}
PID	0.11	0.00033
Cascade	0.10	0.00032
Cascade+RBF	0.071	0.00012

VI. CONCLUSION

A mathematical model of tension loop and speed loop is established based on the dynamic characteristics of the unwinding process of the diaphragm slitting machine, taking the linear speed of the pulling roll as the reference speed. To address the tension fluctuation problem in the unwinding process, a cascade control method combining the sliding mode control algorithm and RBF network adaptive sliding mode control algorithm is proposed. By adding a speed controller with a shorter lag and faster response, the influence of interference in the system can be reduced or eliminated, minimizing its impact on the unwinding tension and increasing the response speed of the unwinding system. Ultimately, simulation and experimental results on the experimental platform demonstrate that this method has good control performance for web tension under different reference tension and transmission speeds. This method can improve the dynamic performance and anti-interference ability of the equipment under different operating conditions and has practical value in industrial production.

Our future work on the tension control of slitters will focus on improving the control performance further in some harsh conditions, like system start-up or close-down, that is from a static state to accelerate the film transport speed, or from full speed to quickly stop the transportation. We are also planning to develop some data-based intelligent algorithms to facilitate the operation of the machine, including online learning algorithms for continuously improving system performance during the machine's lifetime, intelligently prompting system states, pre-caution of possible errors, etc.

REFERENCES

[1] H. Hwang, J. Lee, S. Eum, and K. Nam, "Kalman-filter-based tension control design for industrial roll-to-roll system," *Algorithms*, vol. 12, no. 4, p. 86, Apr. 2019, doi: 10.3390/a12040086.

[2] C. Jiang, H.-S. Wang, L.-W. Hou, and L.-L. Jiang, "Sliding mode compensation control for diaphragm tension in unwinding process of lithium battery diaphragm slitting machine," *IEEE Access*, vol. 8, pp. 21302–21313, 2020, doi: 10.1109/ACCESS.2019.2945976.

[3] P. D. Mathur and W. C. Messner, "Controller development for a prototype high-speed low-tension tape transport," *IEEE Trans. Control Syst. Technol.*, vol. 6, no. 4, pp. 534–542, Jul. 1998, doi: 10.1109/87.701350.

[4] H. Koc, D. Knittel, M. de Mathelin, and G. Abba, "Modeling and robust control of winding systems for elastic webs," *IEEE Trans. Control Syst. Technol.*, vol. 10, no. 2, pp. 197–208, Mar. 2002, doi: 10.1109/87.987065.
[5] Z. Chen, B. Qu, B. Jiang, S. R. Forrest, and J. Ni, "Robust constrained tension control for high-precision roll-to-roll processes," *ISA Trans.*, vol. 136, pp. 651–662, May 2023, doi: 10.1016/j.isatra.2022.11.020.
[6] P. R. Pagilla, N. B. Siraskar, and R. V. Dwivedula, "Decentralized control of web processing lines," *IEEE Trans. Control Syst. Technol.*, vol. 15, no. 1, pp. 106–117, Jan. 2007.
[7] K. C. Lin, "Observer-based tension feedback control with friction and inertia compensation," *IEEE Trans. Control Syst. Technol.*, vol. 11, no. 1, pp. 109–118, Jan. 2003, doi: 10.1109/TCST.2002.806464.
[8] L.-J. Jianga and H. Zhang, "Sensorless parameter adaptive tension control method of winding yarns," *J. Textile Res.*, vol. 43, no. 4, pp. 167–173, 2022.
[9] F. L. Lewis, "Neural network control of robot manipulators," *IEEE Expert*, vol. 11, no. 3, pp. 64–75, Jun. 1996, doi: 10.1109/64.506755.
[10] J. Li, X. Mei, T. Tao, and S. Liu, "Design tension controller of unwinding system based on BP neural network," *Adv. Sci. Lett.*, vol. 4, no. 6, pp. 2222–2226, Jul. 2011, doi: 10.1166/asl.2011.1580.
[11] J. -J. Mi, J. -Y. Yao, and W. -X. Deng, "Neural network based RISE control of winding tension," *J. Mech. Eng.*, vol. 57, no. 24, p. 74, 2021, doi: 10.3901/JME.2021.24.074.
[12] X. Yang, W. Deng, and J. Yao, "Neural adaptive dynamic surface asymptotic tracking control of hydraulic manipulators with guaranteed transient performance," *IEEE Trans. Neural Netw. Learn. Syst.*, vol. 34, no. 10, pp. 1–11, Oct. 2022, doi: 10.1109/TNNLS.2022.3141463.
[13] X. Yang, W. Deng, and J. Yao, "Neural network based output feedback control for DC motors with asymptotic stability," *Mech. Syst. Signal Process.*, vol. 164, Feb. 2022, Art. no. 108288, doi: 10.1016/j.ymssp.2021.108288.
[14] G. Chen and J. Dong, "Approximate optimal adaptive prescribed performance control for uncertain nonlinear systems with feature information," *IEEE Trans. Syst. Man, Cybern. Syst.*, vol. 54, no. 4, pp. 2298–2308, Apr. 2024, doi: 10.1109/TSMC.2023.3342854.
[15] L. Liu, L. Zhou, R. -Y. Deng, and Y.-M. Fang, "Nonsingular fast terminal sliding mode control for the speed and tension system of cold strip rolling mill based on Hamilton theory," *Control Theory Appl.*, vol. 39, no. 5, pp. 857–866, 2022.
[16] J.-S. Lu, M.-Y. Cheng, K.-H. Su, and M.-C. Tsai, "Wire tension control of an automatic motor winding machine—An iterative learning sliding mode control approach," *Robot. Comput.-Integr. Manuf.*, vol. 50, pp. 50–62, Apr. 2018, doi: 10.1016/j.rcim.2017.09.003.
[17] Y. Fang, L. Liu, J. Li, and Y. Xu, "Decoupling control based on terminal sliding mode and wavelet network for the speed and tension system of reversible cold strip rolling mill," *Int. J. Control*, vol. 88, no. 8, pp. 1630–1646, Aug. 2015, doi: 10.1080/00207179.2015.1012119.
[18] L. Yang, L. Mingyong, Z. Xiaojian, and P. Xingguang, "Global approximation based adaptive RBF neural network control for supercavitating vehicles," *J. Syst. Eng. Electron.*, vol. 29, no. 4, pp. 797–804, Aug. 2018, doi: 10.21629/JSEE.2018.04.14.
[19] J. Zhan, Z.-H. Deng, B. Zhu, T.-T. Chang, and Z.-C. Chen, "Sliding mode control based on RBF network for hydraulic pressure in electric power-assisted brake system," *J. Mech. Eng.*, vol. 56, no. 24, p. 106, 2020, doi: 10.3901/JME.2020.24.106.
[20] H. Ding, S. Liu, Z. Li, Z. Wang, and C. Kang, "Design controller based on RBF neural network for the rewinding tension system," in *Proc. IEEE 6th Inf. Technol. Mechatronics Eng. Conf. (ITOEC)*, vol. 6, Mar. 2022, pp. 1448–1452, doi: 10.1109/ITOEC53115.2022.9734603.
[21] Z. Wang, S. Zhu, Q. Chen, X. Zhang, and Y. Song, "Sliding mode control of electro-hydraulic servo system for lower-limb exoskeleton based on RBF neural network," in *Proc. IEEE 10th Conf. Ind. Electron. Appl. (ICIEA)*, Jun. 2015, pp. 79–83, doi: 10.1109/ICIEA.2015.7334088.
[22] X.-M. Xu, W.-X. Zhang, X.-L. Ding, M. Zhang, and S.-H. Wei, "Design and analysis of a novel tension control method for winding machine," *Chin. J. Mech. Eng.*, vol. 31, no. 1, p. 101, Dec. 2018, doi: 10.1186/s10033-018-0304-8.
[23] T. Xiong, G. Zhou, and D. Zou, "State feedback decoupling control of web tension, velocity and lateral displacement in unwinding system," in *Proc. Chin. Control Decis. Conf. (CCDC)*, Aug. 2020, pp. 5217–5224, doi: 10.1109/CCDC49329.2020.9164261.
[24] Y. Yang, W. Cao, Z. Cao, H. Zhou, F. Gao, and J. Shi, "Integrated design method of a cascade iterative learning control for the cascaded batch/repetitive processes," *Ind. Eng. Chem. Res.*, vol. 55, no. 6, pp. 1598–1608, Feb. 2016, doi: 10.1021/acs.iecr.5b02489.
[25] L. Liu, Y. -M. Fang, X. -G. Li, and J. -X. Li, "Tensiometer-free control for a speed and tension system of reversible cold strip mill based on Hamilton theory," *Acta Automatica Sinica*, vol. 41, no. 1, pp. 165–175, 2015.
[26] Q. Hong, Y. Shi, and Z. Chen, "Dynamics modeling and tension control of composites winding system based on ASMC," *IEEE Access*, vol. 8, pp. 102795–102810, 2020, doi: 10.1109/ACCESS.2020.2997340.

LIANG WANG received the B.E. degree in mechanical engineering from Hohai University, Changzhou, China, in 2008, and the M.E. degree in mechanical engineering from Nanchang Hangkong University, Nanchang, China, in 2011. He is currently pursuing the Ph.D. degree in mechatronics engineering with the College of Mechanical and Electrical Engineering, Central South University, Changsha, China. His current research interest includes modeling and control of electromechanical systems.

HENGSHENG WANG received the Ph.D. degree in mechanical and electrical engineering from Central South University (CSU), Changsha, China, in 2006. He is currently a Professor with the College of Mechanical and Electrical Engineering, CSU. His research interests include dynamics and control of mechanical systems, industrial manipulators, mobile robotics, and the applications of artificial intelligence.

ZHOU OUYANG received the B.E. degree in mechanical engineering from Changsha University of Science and Technology, Changsha, China, in 2019, and the M.E. degree in mechanical engineering from Central South University, Changsha, China, in 2022, where he is currently pursuing the Ph.D. degree in mechatronics engineering with the College of Mechanical and Electrical Engineering. His research interests include automatic control and research of control algorithm.

HUA LIU received the bachelor's degree in mechanical engineering from Inner Mongolia University of Technology, Hohhot, China, in 2017, and the master's degree in mechanical engineering from Taiyuan University of Technology, Taiyuan, China, in 2020. He is currently pursuing the Ph.D. degree in mechanical engineering with the College of Mechanical and Electrical Engineering, Central South University, Changsha, China. His research interests include hydraulic manipulator control and motion planning.

ZEXING ZHENG received the B.E. degree in mechanical engineering from Central South University, in 2021, where he is currently pursuing the M.E. degree in mechanical engineering. His research interest includes modeling and control of electromechanical systems.